JOURNAL OF GEOPHYSICAL RESEARCH, VOL. , NO. , PAGES 1–9,

# Barrier Layer Formation During Westerly Wind Bursts

Meghan F. Cronin and Michael J. McPhaden

NOAA/Pacific Marine Environmental Laboratory, Seattle, WA, USA

**Abstract.** Barrier layers between the base of a shallow halocline and the top of the thermocline are a common feature of the western Pacific warm pool. In this paper, we investigate barrier layer formation and erosion processes associated with two westerly wind bursts (WWBs). WWBs are typically associated with increased rainfall, but increased wind stirring and convective mixing from surface cooling can cause the freshwater to mix down to the top of the thermocline and thereby erode pre-existing or newly formed barrier layers. However, not all WWBs lead to barrier layer erosion. In this study we show that a WWB in November 1989 was associated with the formation of an extremely (∼100 m) thick barrier layer. During this event, zonal and meridional advection of surface freshwater from the west and north were the dominant processes responsible for the thick barrier layer, while rainfall was a secondary process. Likewise during the Coupled Ocean Atmosphere Response Experiment (COARE), a relatively thick barrier layer formed near 0°, 160°E and 0°, 165°E following the October 1992 WWB. Zonal convergence associated with this WWB caused a zonal salinity gradient to intensify. The surface intensified wind-driven jet then tilted the zonal salinity gradient into the vertical, thus generating a shallow halocline above the top of the thermocline. In both events, feedbacks appear to have occurred between formation of stratification and formation of vertical shear. Shear formed through a depth dependent pressure gradient associated with the salinity gradient and through trapping of wind-forced momentum above the developing stratification. The increased sheared flow then led to further surface-intensified freshwater advection and stratification. These examples illustrate how, in the presence of zonal and meridional salinity gradients, the equatorial ocean's response to WWBs can include the formation of thick, long-lived barrier layers.

## 1. Introduction

Throughout much of the world's oceans, upper ocean density stratification is controlled primarily by temperature. In the western equatorial Pacific, however, surface stratification defining the base of the mixed layer is often controlled by salinity and the mixed layer can be significantly shallower than would be expected based upon the temperature stratification. The salinity stratified isothermal layer between the base of the mixed layer and top of the thermocline is often referred to as the "barrier layer" [*Godfrey and Lindstrom*, 1989] since it acts as a barrier to turbulent entrainment of cold thermocline water into the surface mixed layer. Although barrier layers are a climatological feature of the western equatorial Pacific [*Sprintall and Tomczak*, 1992], they have substantial spatial and temporal variability. In this study we investigate barrier layer formation and erosion processes associated with westerly wind bursts.

Barrier layer formation mechanisms fall into two broad classes: local surface processes (e.g., rain under low wind conditions) and subduction and advection processes. Westerly wind bursts (WWBs) tend to occur during the convective phase of the intraseasonal Madden Julian Oscillation (MJO) and therefore are often associated with heavy rainfall and surface cooling [*Madden and Julian*, 1994]. Thus, because MJO rainfall occurs in concert with increased turbulent mixing, *Zhang and McPhaden* [2000] found that the westerly phase of the MJO tended to be associated locally with barrier layer thinning rather than its growth, based on moored data from 1991–1994. Local rain-formed fresh surface lenses tend to produce relatively thin barrier layers [*You*, 1995; *Soloviev and Lukas,* 1996; *Vialard and Delecluse*, 1998a,b] that dissipate within several days of the rain event [*Wijesekera and Gregg*, 1996; *Smyth et al.*, 1997; *Wijesekera et al.*, 1999].

Recognizing that the eastern portion of the Pacific warm pool was a region of large-scale convergent flow associated with the termination of the mean trade winds, *Lukas and Lindstrom* [1991] hypothesized that the climatological barrier layer near the dateline was caused by subduction of salty, warm South Equatorial Current water beneath fresh, warm pool water. The zonal subduction mechanism for forming barrier layers was demonstrated by *Vialard and Delecluse* [1998a,b] using an OGCM with realistic daily forcing for the period 1984–1993. The OGCM formed a sea surface salinity (SSS) front between the fresh warm pool and the salty South Equatorial Current. Thick barrier layers were associated with zonal convergence and subduction in the SSS frontal zone. In contrast, when there was no significant barrier layer in the SSS frontal region, there tended to be no surface eastward fresh jet and upwelling prevailed throughout the region. On interannual time scales, the OGCM SSS front and region of thick barrier layer shifted zonally in qualitative agreement with barrier layer thickness calculations based on CTD data [*Ando and McPhaden*,



Paper number .
0148-0227/02/$9.00

1997]. Although meridional SSS gradients and convergence can be strong on and near the equator, meridional subduction and advection have not been explored as a barrier layer formation mechanism.

The dynamical equatorial ocean response to westerly wind bursts typically includes surface eastward acceleration [*Yoshida*, 1959], Ekman surface meridional convergence and downwelling on the equator, and a spectrum of equatorial waves [*Moore and Philander*, 1977]. Further, *Cronin et al.* [2000] showed that the equatorial ocean adjusts rapidly to wind forcing by setting up a compensating pressure gradient that forces a subsurface jet in the direction opposing the winds. In particular, westerly wind bursts set within a background of easterly trades can give rise to vertically stacked currents, with eastward flow at the surface and westward flow within the upper portion of the thermocline, above the eastward Equatorial Undercurrent. Thus, westerly wind burst forcing can cause vertical shears, horizontal convergences, and downwelling, all of which, as we show in the following section, can be important ingredients in the formation of barrier layers.

## 2. Barrier Layer Formation Mechanisms

In order to provide a mathematical framework for barrier layer analyses, we begin with a review of the mechanics by which near-surface stratification can form. Barrier layers require the near surface density stratification $\rho_z$ to be controlled by salinity stratification $S_z$, rather than temperature stratification $T_z$, i.e.,

$$\rho_z = \frac{\partial \rho}{\partial T} T_z + \frac{\partial \rho}{\partial S} S_z \sim \frac{\partial \rho}{\partial S} S_z, \tag{1}$$

where $\partial\rho/\partial T$ and $\partial\rho/\partial S$ are respectively the partial derivatives of density with respect to temperature and salinity. To understand how surface salinity stratification can develop, we take the vertical derivative of the salinity balance, i.e.:

$$\begin{aligned} S_{zt} = \; & \underset{1}{-\mathbf{U} \bullet \nabla S_z} \;\; \underset{2}{-w S_{zz}} \;\; \underset{3}{-\mathbf{U}_z \bullet \nabla S} \\ & \underset{4}{-w_z S_z} \;\; \underset{5}{-(\overline{w'S'})_{zz}}, \end{aligned} \tag{2}$$

where $\boldsymbol{U}$ is the horizontal velocity, $w$ is the vertical velocity, $\nabla$ is the horizontal gradient operator, and $\overline{w'S'}$ is the vertical turbulent flux of salinity. Note that at the air-sea interface ($z = 0$) the turbulent salinity flux depends upon evaporation ($E$) and precipitation ($P$) according to:

$$\overline{w'S'}\Big|_{z=0} = S_0(E - P), \tag{3}$$

where $S_0$ is the surface salinity. Thus surface forcing is contained within the turbulent mixing component (term 5) of (2).

A similar equation can be developed for temperature stratification:

$$\begin{aligned} T_{zt} = \; & \underset{1}{-\mathbf{U} \bullet \nabla T_z} \;\; \underset{2}{-w T_{zz}} \;\; \underset{3}{-\mathbf{U}_z \bullet \nabla T} \\ & \underset{4}{-w_z T_z} \;\; \underset{5}{-(\overline{w'T'})_{zz}} \;\; \underset{6}{+\frac{1}{\rho c_p}(Q_{rad})_{zz}}, \end{aligned} \tag{4}$$

where $\rho c_p$ is the volumetric heat capacity, $Q_{rad}$ is the penetrative solar radiation, and $\overline{w'T'}$ at $z = 0$ is proportional to the net surface heat flux reduced by the solar radiation at the surface. Often the corresponding terms in (2) and (4) are correlated. For example, rainfall is correlated with reduced solar warming and increased surface cooling, temperature advection is often correlated with salinity advection; downwelling affects both temperature stratification and salt stratification. Thus, when analyzing the formation of barrier layers, one must consider not only processes governing salinity stratification, but also how these occur without generating a corresponding temperature stratification.

Figure 1 illustrates kinematics of barrier layer formation and growth corresponding to terms 1, 3, 4, and 5 in (2) and (4). A barrier layer can be advected into a region (term 1) if the barrier layer thickens (e.g., if the halocline shoals relative to the thermocline) in the direction from which the water flows. Likewise, as shown in Figure 1, a barrier layer can form when a vertically sheared horizontal flow advects a horizontal salinity gradient within the isothermal surface layer (term 3). This causes near-vertical salinity contours to tilt into the horizontal, thus generating a shallow halocline above the top of the thermocline. Vertical advection acting uniformly on both the halocline and thermocline (term 2) will cause the barrier layer to shift vertically, with no change in the barrier layer's thickness. Thus, vertical advection of a barrier layer is not illustrated in Figure 1. However, if the vertical velocity acts non-uniformly on the two depth surfaces, then the barrier layer can grow through vertical stretching (term 4). Finally, rainfall, in the absence of strong turbulent mixing and surface heating, can cause a barrier layer to form between the base of the rainwater puddle (fresh lens) and the top of the thermocline (term 5).

Note that feedbacks can develop between formation of stratification and changes in the horizontal currents. In particular, as stratification increases, turbulent mixing tends to decrease based on Richardson number arguments. Consequently, surface generated momentum (e.g., wind forced surface jets) can become trapped above the newly formed stratification, causing shears to develop above the top of the thermocline. The resulting sheared flow can then cause further stratification through the tilting process (term 3 in (2) and (4)). Alternatively, vertically sheared flow that tilts contours into more vertical orientation will cause a reduction in the stratification. Ultimately, the water column can become gravitationally unstable (dense water overlying lighter water), generating turbulence through convective overturning. The net effect of tilting in this case is dissipation of the horizontal and vertical salinity gradient. Finally, as discussed in the Appendix and by *Roemmich et al.* [1994], a zonal salinity gradient can give rise to velocity shear within the mixed layer through a depth dependent pressure gradient. This sheared zonal flow can then tilt the zonal salinity gradient into the vertical and thus form salinity stratification above the top of the thermocline. The ocean's response to wind and buoyancy forcing can thus be quite complex.

A complete quantitative analysis of the processes governing barrier layer formation and erosion (i.e., equations 2 and 4) requires information on the three-dimensional structure of the upper ocean temperature and salinity fields, three-dimensional flow and its vertical shear, local surface forcing, and turbulent mixing profile. Because we have a more limited data set, a quantitative analysis is beyond the scope of this paper. These equations, however, provide guidance for assessing processes responsible for changes in the observed barrier layer thickness described in the following sections.

## 3. Barrier Layer Calculation

In this analysis we use data from Tropical Atmosphere Ocean (TAO) moorings enhanced with Seabird Electronics conductivity and temperature (SEACAT) sensors to compute a multi-year, daily time series of barrier layer thickness in the western equatorial Pacific. These moorings include the TAO current meter mooring at 0°, 165°E from 1989 through mid-1994, COARE ATLAS moorings at 0°, 154°E and 0°, 160.5°E from mid-1992 through early 1993, and the COARE-enhanced TAO mooring at 0°, 156°E from mid-1991 through mid-1994. For more information on TAO moorings, see *McPhaden et al.* [1998]. For details on SEACAT temperature and salinity data, see *Sprintall and McPhaden* [1994], *Cronin and McPhaden* [1998], and *Freitag et al.* [1999].

Following *Sprintall and Tomczak* [1992], we define isothermal layer depth ($MLD_T$) in terms of a temperature step $\Delta T$ from the sea surface temperature $T_s$, and mixed layer depth ($MLD$) in terms of density step $\Delta\rho$, equivalent to $\Delta T$, from the sea surface density $\rho_s$:

$$MLD_T = z(T = T_s + \Delta T) \tag{5}$$

$$MLD = z(\rho = \rho_s + \frac{\partial \rho}{\partial T}\Delta T). \tag{6}$$

The difference between these two surfaces is the barrier layer thickness ($BLT$):

$$BLT = MLD - MLD_T. \tag{7}$$

Thus, if there is no salinity stratification and density stratification is controlled entirely by temperature, then the mixed layer depth (6) is equivalent to the isothermal layer depth (5) and the barrier layer thickness (7) is zero.

For most deployments, the top SEACAT was at 1 m or 3 m depth. Thus, for consistency, $T_s$ and $\rho_s$ in (5) and (6) were 3 m depth temperature and density (except prior to November 1989, when 10 m values are used). $\partial\rho/\partial T$ was computed based on observed surface temperature and salinity. Daily averaged data were used in (5)–(7), and therefore, following *Cronin and Kessler* [2002], we chose a temperature step that was larger than the diurnal cycle amplitude of the 3 m surface value. Large diurnal variations in temperature are limited to the top several meters [*Anderson et al.*, 1996]. On average, at 1 m, the peak-to-peak amplitude is 0.4°C, while at 3 m, the amplitude is reduced by a factor of two [*Cronin and McPhaden*, 1999]. We therefore chose $\Delta T$ to be –0.25°C. For a mixed layer within a constant temperature layer, this $\Delta T$ corresponds to a salinity step of 0.11 psu, well within the SEACAT sensor measurement error. After post-processing, salinity measurement error is approximately 0.02 psu [*Freitag et al.*, 1999]. Temperature measurement errors are 0.01°C for SEACATs and 0.01–0.09°C for other TAO temperature sensors. The MLD error therefore depends primarily upon the vertical resolution of the sensors. Barrier layer thicknesses which are less than the sensor spacing should be viewed with caution.

Daily BLT time series, filtered with a 15-day Parzen filter, are shown in Figure 2 in relation to the *Reynold and Smith* [1994] weekly SST and the *Delcroix et al.* [2000] monthly gridded SSS fields. Gridded SSS data originate from a compilation of data by *Institut de Recherche pour le Développement* (IRD) that included bucket measurements from ship-of-opportunity, hydrocast and CTDs collected during research cruises, thermosalinographs installed on merchant and research vessels, and from TAO moorings (as described above). Data were tested for outliers, then optimally interpolated onto a monthly, 2° latitude by 10° longitude grid centered on the equator at 145°E, 155°E, 165°E, etc. [*Delcroix et al.*, 1996].

Consistent with the results of the CTD-only barrier layer thickness calculations of *Ando and McPhaden* [1996] (AM), the barrier layer is thickest near the large-scale SSS front associated with the eastern edge of the warm/fresh pool (Figure 2). The warm/fresh pool exhibits substantial interannual variability, shifting eastward during El Niño warm events and westward during La Niña cool events. As in the AM CTD-only analysis, thick (>30 m) barrier layers were found at 0°, 165°E through the end of 1989 and much of 1990. The COARE enhanced monitoring period (August 1991–April 1994), however, was a period of generally thin or no barrier layers, with the exception of a barrier layer near 160°E and 165°E toward the end of 1992 and beginning of 1993, and a developing thick barrier layer at 156°E beginning in 1994 (both this analysis and the AM analysis end in mid-1994). Although coverage is not as good and gaps exist, the moored BLT time series has better time resolution than the CTD-only analysis, and thus can be used to analyze the role of WWBs.

The evolution of BLT in relation to wind and rainfall variability is shown in Figure 3. TAO gridded winds shown here are 2°N, 0°, 2°S averaged zonal winds, 5-day averaged and sub-sampled, and filtered with a 1-2-1 filter. Rain rates are from *Xie and Arkin* [1997]. Note that westerly winds are typically associated with rain rates in excess of 15 mm day$^{-1}$. These convective patterns typically begin in the far western Pacific and propagate eastward to the edge of the warm pool leaving cooler, fresher water in their wake (Figures 2–3). WWB rainfall and surface heat fluxes tend to both enhance the large-scale zonal SSS gradient and reduce the large-scale zonal SST gradient on the eastern edge of the warm pool.

As shown in Figure 3, WWB are often associated with barrier layer thinning, consistent with the results of *Zhang and McPhaden* [2000]. Several WWB, however, clearly led to barrier layer formation. Indeed, the thickest barrier layer in the entire record (Figure 3) appears to have formed in response to the well-documented WWB in November 1989 [*McPhaden et al.*, 1992] (M92). As described by M92, the November 1989 WWB occurred during an intensive oceanographic survey centered near 0°, 165°E, involving hydrographic transects, drifter deployments, and moored measurements. This event, therefore, is the subject of our first case study.

## 4. Case Studies

### 4.1. Barrier Layer Formation During the November 1989 WWB

The November 1989 WWB followed an extended period of strong easterlies associated with the 1988–1989 La Niña (Figures 2–3). As is typical of La Niña cold events, during most of 1989, the warm/fresh pool was confined to the far western Pacific, west of 0°, 165°E. However, during the November 1989 WWB, warm pool SST cooled and the eastern edge of the warm/fresh pool shifted eastward, so that by December 1989 the 29°C SST was found near the date

line. The November 1989 WWB thus marks the transition from La Niña cold conditions to normal conditions.

As shown in Figure 4, zonal surface currents at 0°, 165°E became eastward on November 20, about a day before local winds became westerly. Within less than a week (by November 26), westerly winds had speeds of 8 m $s^{-1}$, 10 m zonal currents were eastward at 1 m $s^{-1}$, the thermocline had deepened to ∼150 m, and SST had cooled by more than 0.3°C. Because of rapid near-surface freshening (1.2 psu in 10 days above 40 m) and weaker subsurface freshening (0.6 psu in 5 days between 40 m and 100 m), a halocline formed near 40 m. Thus, while $MLD_T$ deepened, MLD remained near 40 m, forming a 100 m thick barrier layer.

In contrast to this increased salinity stratification, the combination of surface cooling and subsurface warming between 40 m and 150 m caused a reduction in the upper ocean's thermal stratification. For nearly 2 weeks (November 27–December 8), the thick barrier layer supported a temperature inversion of about 0.2°C. The barrier layer was both thick and long-lasting. Five months after its formation, the barrier layer was still nearly 30 m thick (Figures 2–3).

Nearly all processes listed in (2) and (4) appear to have been in action during this event. Between November 10–29, rainfall accumulation was ∼307 mm, with up to pentad averaged rates of 22 mm $day^{-1}$ (Figure 4d). This amount of freshwater distributed over 40 m would cause a freshening of only 0.3 psu, while the observed change was nearly 1 psu. Thus, there must have been other sources of freshwater besides local rainfall.

The gridded SSS fields (Figure 2) and the CTD sections (M92's Figure 9) show that prior to the WWB substantially fresher ($\lesssim$34.0 psu) water could be found west of 155°E along the equator and near 4°N along 165°E. Both of these fields indicate large horizontal gradients in these regions of order 1 psu/1000 km zonally and 1 psu/300 km meridionally. In contrast, warmest waters were found near 160°E along the equator and south of 4°S along 165°E (see M92's Figure 14), so that the zonal SST gradient was roughly –0.4°C/500 km between 165°E and 160°E and +0.2°C/1000 km between 155°E and 145°E, while the meridional SST gradient was roughly –0.2°C/200 km south of the equator and negligible north of the equator. In other words, horizontal density gradients were dominated by salinity gradients during this event.

Although flow at 0°, 165°E had been eastward for only a couple of days prior to the freshening, the deepening thermocline and zonal current reversal at 0°, 165°E suggest there was strong horizontal convergence in this region. And, since westerly winds at 155°E occurred more than a week prior to the westerlies at 165°E, it is likely that flow was eastward, west of 165°E prior to the current reversal at 0°, 165°E. Because horizontal convergence can cause a property gradient to become front-like, it is plausible that the zonal salinity gradient was locally larger than 1 psu/1000 km during the rapid freshening. If in fact the SSS gradient was 0.2 psu/100 km, then advection by a 50 cm $s^{-1}$ current could cause 0.2 psu freshening in 2 days (about half the observed change between November 21–23); while the average 75 cm $s^{-1}$ eastward current advecting a 1 psu/1000 km for 10 days would cause a 0.6 psu freshening (again, about half the observed change).

During the rapid freshening, meridional surface currents were first weakly northward and then became 20–40 cm $s^{-1}$ southward on November 23. A 30 cm $s^{-1}$ southward current advecting a 1 psu/300 km gradient for 7 days could also cause a 0.6 psu freshening. Thus, observed 1.2 psu surface freshening in 10 days could be accounted for by a combination of zonal and meridional advection and rainfall.

Below 40 m, there was weaker freshening, with rapid freshening at 100 m depth occurring ∼5 days after the freshening at the surface. Such a delay could be achieved through uniform advection of a tilted front (term 1 in (2)) by a 40 cm $s^{-1}$ current if the front was tilted ∼175 km zonally over the top 100 m. Alternatively, through term 3 in (2), a horizontal front 0.2 psu/100 km could be tilted into a vertical stratification 0.2 psu/50 m in 3 days, if the current had a shear of 40 cm $s^{-1}$ over the top 50 m. Such a shear was observed between the 10 m and 50 m current meters November 22–25. Finally, if Ekman downwelling increased with depth between the surface and the top of the thermocline, then vertical stretching between the deepening $MLD$ and $MLD_T$ (term 2 in (2)) could have caused the barrier layer to thicken. Thus, barrier layer formation at 0°, 165°E during the November 1989 WWB is consistent with tilting of a zonal and meridional gradient into the vertical through advection by a sheared flow (term 3 in (2)), advection of the remotely tilted front into the region (term 1 in (2)), and rainfall (term 6 in (2)). Further, thermocline downwelling likely increased the thickness of the barrier layer (term 2 in (2)).

### 4.2. Barrier Layer Formation During the October 1992 WWB

To further investigate the role of the large-scale gradients and the formation of barrier layers during different phases of El Niño/Southern Oscillation, in this second case study we focus on a relatively thick barrier layer that formed in response to the October 1992 WWB (Figures 2–3 and the corresponding Figure 5). This WWB occurred amidst extended El Niño warm conditions of the early 1990s (Figures 2–3). Because the COARE intensive observational period began during this event, the October 1992 WWB is also well documented. For analyses of the upper ocean heat, salt, and zonal momentum budgets at 0°, 156°E, see, respectively, *Cronin and McPhaden* [1997, 1998] and *Cronin et al.* [2000]. See *Helber and Weisberg* [2001] for analysis of the vertical velocity at 0°, 156°E during this event. For analysis of the convection pattern associated with this WWB and its relation to the MJO intra-seasonal oscillation, see *Godfrey et al.* [1998].

In addition to enhanced salinity monitoring (described earlier in Section 3), during COARE an array of moored ADCPs monitored the upper ocean currents along the equator at 154°E, 156°E, 157.5°E, and 165°E. The start and end dates and top and bottom bins are listed in Table 1 of *Cronin et al.* [2000]. A large number of CTD casts were also made in the vicinity of the moorings. In order to compute dynamic height relative to 500 m, *Cronin et al.* [2000] combined CTDs with SEACAT measurements to create a daily T-S curve at each site. With these curves, salinity could be computed based upon the temperature measurements. At and above the bottom SEACAT depth, daily averaged salinity are identical to the SEACAT measurements. However, below the bottom SEACAT depth, the T-S curve reverts to the slowly varying curve measured by the CTDs and nearby 0°, 156°E and 165°E moorings. These deeper salinity fields are shown in the zonal section in Figure 6, but were not used to estimate the barrier layer thickness.

As shown in Figures 2–3 and 5, the barrier layer formation event during the October 1992 WWB differed from the dramatic November 1989 barrier layer formation event. For one, it was thinner (∼60 m thick versus ∼100 m thick). Also, while warmest waters were to the west of 165°E during the November 1989 event, during the October 1992 event, the warm pool extended to near the dateline and the warmest waters were to the east of the study region. In both cases fresher water was to the west. Thus, during the October 1992 WWB, the salinity gradient near 0°, 156°E coincided with a density compensating temperature gradient. Notice also that the zonal SSS gradient's extension into the COARE study region during the latter half of October 1992 is not resolved in the monthly gridded fields shown in Figure 2.

Westerly winds and heavy rainfall first appeared in the far western Pacific in mid-October and then extended eastward to near 170°E by the last week of October 1992. As easterlies shifted to westerlies at 154°E and 156°E in mid-October, winds became very weak. However, despite weak winds and high rainfall, no barrier layer formed at these sites (Figure 5). Relatively thick barrier layers formed at 160.5°E and 165°E at the end of October, as the SSS front began to move eastward across these sites.

Figure 6 shows the zonal current pattern relative to the subsurface temperature and salinity fields for the 5-day period in which the barrier layer formed (October 27–November 1, 1992). Subsurface zonal convergence near 156°E was coincident with the maximum zonal temperature and salinity gradients (Figure 6). While these SST and SSS gradients were probably caused by zonal patterns of surface forcing, it is likely that zonal convergence helped tighten zonal gradients near 156°E. However, because the positive SST gradient often dominated over the somewhat density compensating positive SSS gradient at 0°, 156°E, advection by sheared flow tended to cause neutral or even possibly convectively unstable stratification. It is likely that the resulting enhanced turbulent mixing at 156°E contributed to the deep MLD, near-uniform flow, and isotherms and isohalines that were near-vertical in the zonal-vertical plane (Figure 6) at that site.

East of 0°, 157.5°E, however, the zonal SST gradient was weak and the density gradient was controlled by salinity. At 157.5°E there was indication of vertically sheared eastward flow. At 165°E the surface-intensified flow had a 0.2 m $s^{-1}$ shear between 10 m and 60 m, with eastward flow above 30 m and westward flow below. Although too weak by a factor of 2, this shear was of the correct sign to produce stable stratification through the tilting mechanism. Thus, it is likely that the tilting term in (2) played a role in the barrier layer formation at 160.5°E and 165°E. However, the apparent large tilt in the isohalines between 160.5°E and 165°E (∼50 m in 450 km) likely was caused by a combination of processes. For comparison, during the November 1989 event the estimated tilt was 50 m in 100 km. While the halocline (i.e., mixed layer) was very shallow at 165°E, the thermocline was deep and there was a weak temperature inversion within the barrier layer (Figure 6).

## 5. Discussion

Using COARE-enhanced mooring data from 1991 to 1994, *Zhang and McPhaden* [2000] showed that the convectively active phase of the MJO tended to be associated locally with westerly winds, increased wind speed, rainfall, surface heat loss, SST cooling, and barrier layer thinning. Some WWB, however, are quite effective at forming thick barrier layers, as shown in Figure 3. These barrier layers tended to be in regions with large horizontal salinity gradients (Figure 2). Therefore, to complement the *Zhang and McPhaden* [2000] local analysis, in this study we have focused on how WWB advective processes can contribute to barrier layer formation. In particular, we have identified the "tilting" mechanism acting on both zonal and meridional salinity gradients to be critical to the formation of thick barrier layers during WWB.

Barrier layers form when a halocline develops above the top of the thermocline. The tilting mechanism occurs when a vertically sheared horizontal flow, advecting a horizontal salinity gradient, tilts the horizontal salinity gradient into a vertical stratification. When this process occurs within the isothermal layer above the top of the thermocline, a barrier layer can form. In *Lukas and Lindstrom*'s [1991] subduction hypothesis for climatological barrier layer, zonal tilting is accomplished by a subsurface westward flow that carries salty warm water below the fresh warm pool water. However, while subsurface westward currents are often observed in response to westerly wind bursts [*Cronin et al.*, 2000], these transient subsurface westward currents are typically within the upper portion of the thermocline, rather than within the isothermal layer above the thermocline (see Figure 4 and 6). Transient westward currents in the thermocline may play a role in providing a source of salty water that maintains the barrier layer. However, they are not active in the tilting process within the isothermal layer. Instead, our analysis shows that during WWB, zonal tilting occurs through surface intensified freshwater advection, i.e., through an eastward ("Yoshida") jet acting on the eastern edge of the fresh pool. Once formed, the barrier layer can thicken through vertical stretching, if WWB Ekman downwelling increases with depth within the barrier layer.

In previous barrier layer analyses, the role of meridional advection was not addressed. We found, however, that during the November 1989 WWB, meridional tilting was as important as zonal tilting in forming the very thick barrier layer. Meridional surface Ekman convergence is a robust feature of WWBs [*McPhaden et al.*, 1988, 1992; etc.]. As shown by *Hénin et al.* [1998] and *Ioualalen and Hénin* [2001], the meridional SSS gradient can have large interannual variability, similar to the zonal SSS gradient. During La Niña events, the warm/fresh pool is confined to the far western Pacific, and rainfall is limited to the ITCZ in the northern hemisphere. Consequently, La Niña are often associated with a large meridional SSS gradient, with high SSS values on the equator. WWBs tend to freshen surface equatorial waters through enhanced rainfall and by bringing northern hemisphere freshwater toward the equator. That is, WWBs tend to reduce the meridional SSS gradient. Consequently, the first WWB at the end of a La Niña cold event may be most effective at tilting the meridional SSS gradient into vertical salinity stratification. If so, then these WWBs (such as the November 1989 WWB) may be particularly effective at producing thick barrier layers. Further, the reduced entrainment caused by the resulting thick barrier layer may help cause SSTs to warm and the large-scale system to return to normal or warm conditions.

In general, the pattern of WWB rainfall and surface cooling tends to enhance the large-scale positive zonal salinity gradient and reduce the large-scale SST gradient associated

with the eastern edge of the warm/fresh pool. Indeed, during the October 1992 WWB, warmest waters were in the eastern portion of the study region. Between 0°, 154°E and 0°, 157.5°E, the positive SST gradient was large enough that, despite the positive zonal SSS gradient throughout the region, surface water at 0°, 154°E was often slightly denser than at 0°, 156°E. At these sites, the tilting mechanism did not result in a barrier layer; instead, it appears that turbulent mixing extended down to the top of the thermocline. At 0°, 160.5°E and 0°, 165°E, however, there was little SST gradient and surface-intensified freshwater advection contributed to barrier layer formation. The tilting mechanism can either create barrier layers or destroy them depending on the sign of the vertically sheared flow relative to the salinity-controlled density gradient. If the zonal salinity gradient is always positive (salty water to east), then advection by surface-intensified eastward flow will tend to produce barrier layers, and advection by surface-intensified westward flow will tend to destroy them. Since the large-scale SSS gradient is formed by convergence between the eastward fresh jets and westward salty South Equatorial Current, the tilting mechanism will preferentially form barrier layers on the western edge of the large-scale positive zonal salinity gradient as found by *Vialard and Delecluse* [1998b].

Direct wind forced accelerations tend to be trapped within the mixed layer. As near surface stratification develops, flow above the top of the thermocline can become increasingly sheared. Thus a positive feedback can develop between the formation of shear and formation of a shallow halocline. With continued wind forced accelerations, ultimately, sheared flowed instability can develop and erode the stratification, thus terminating the feedback [*Roemmich et al.*, 1994]. The fact that the barrier layers examined here were long-lasting suggests that the feedback terminated before shear flow instability developed. WWB are by their nature variable, typically not lasting more than a month. However, even for sustained winds, direct wind forced accelerations do not continue indefinitely. Instead, typically within a week or so, a pressure gradient develops that counters the wind forcing [*Cronin et al.*, 2000]. These WWB-generated zonal pressure gradients are independent of the *Roemmich et al.* [1994] pressure gradients, which are associated with the zonal salinity gradients (see Appendix). In contrast to the *Roemmich et al.* [1994] pressure gradient, the WWB-generated pressure gradient can prolong the life of the barrier layer by limiting the wind-generated vertical shear, so that the tilting-shear feedback terminates before sheared-flow instability and mixed layer erosion develops. Also, WWB-generated pressure gradients can drive transient subsurface westward currents within the upper thermocline that may extend the life of the barrier layer by supplying a source of salty water that can be entrained into the barrier layer from below. Barrier layers formed during WWB can thus be long-lived.

Perhaps a more interesting question is how the tilting process starts. If the mixed layer initially extended to the top of the thermocline (that is, initially there was no barrier layer), then shear must exist within the mixed layer for the tilting mechanism to operate. Vertically sheared flow can exist within a mixed layer of finite viscosity [e.g., *Stommel*, 1960; *McPhaden et al.*, 1988]. However, an interesting possibility is that the shear in the mixed layer that begins the formation process might be generated by a depth-dependent pressure gradient associated with the zonal salinity gradient [*Roemmich et al.*, 1994]. Scale analysis (see Appendix) during the November 1989 and October 1992 WWB indicates that the zonal SSS gradients could have generated weak shears of the correct sense (e.g., 20 cm $s^{-1}$/50 m in 3 days during the November 1989 formation event, 8 cm $s^{-1}$/50 m in 3 days during the October 1992 event). These shears, therefore, could have provided the impetus for developing larger shears through the tilting of isohalines and the wind momentum trapping/tilting feedback. However, acting alone, the zonal SSS gradients could not generate sufficiently large shear to produce the observed barrier layers. Alternatively, rainfall could cause weak freshwater stratification that could help initiate the positive feedback process.

Unfortunately, even with the enhanced monitoring for these two surveys, a more quantitative analysis cannot be performed. As shown in (2) and (4), to perform a quantitative analysis of barrier layer formation, temperature, salinity and currents must be resolved from the surface through the top of the thermocline. Likewise, because zonal and meridional advection appear to be a critical element of barrier layer formation, horizontal salinity and temperature gradients must be resolved, as well as their variations with depth. Finally, because there is substantial temporal and spatial variability in the formation of barrier layers, these measurement systems must be correctly placed in time and space. During COARE, it is likely that thick barriers formed to the east of the COARE-enhanced monitoring region. Thus, in retrospect, the COARE array of moorings may not have been ideally located for studying barrier layer dynamics.

## Appendix

A zonal salinity gradient within the mixed layer can be associated with a depth dependent zonal pressure gradient ($\partial P/\partial x$) whose vertical derivative within the mixed layer is:

$$-\frac{\partial}{\partial z}\frac{\partial P}{\partial x} = g\frac{\partial \rho_s}{\partial x} \tag{A1}$$

where $g$ is gravity. Thus, as pointed out by *Roemmich et al.* [1994], assuming the pressure gradient remains unbalanced by wind stress, turbulent stress divergence, and non-linear advection terms on the equator, a zonal salinity gradient can give rise to vertical sheared zonal flow within the mixed layer,

$$\frac{\partial}{\partial t}\frac{\partial u}{\partial z} \sim \frac{g}{\rho_0}\frac{\partial \rho}{\partial S}\frac{\partial S}{\partial x} \tag{A2}$$

which can then tilt the horizontal gradient into the vertical via term 3 in (2) and (4). For scale analyses, $g \sim 9.8$ m $s^{-2}$, $(\partial\rho/\partial S)/\rho_0 \sim 7.5 \times 10^{-4}$ psu$^{-1}$, and $(-\partial\rho/\partial T)/\rho_0 \sim 3.3 \times 10^{-4}$ °C$^{-1}$.

Based on (A2), the 0.2 psu/100 km salinity gradient estimated during the November 1989 WWB could cause a depth dependent acceleration of $1.5 \times 10^{-8}$ $s^{-2}$, so that after 3 days the surface current would be 20 cm $s^{-1}$ faster than at 50 m. Thus the *Roemmich et al.* process contributed perhaps up to 50% to the observed shear. It is likely that the large shear observed formed through a combination of wind-forcing and the *Roemmich et al.* depth dependent pressure gradient.

Likewise, assuming no density compensation from a temperature gradient, the observed salinity gradient during the October 1992 WWB (0.8 psu/1000 km) could cause up

to 8 cm $s^{-1}$ shear between the surface and 50 m to develop in 3 days (less than half the observed shear). By (2), this shear could cause the zonal gradient to tilt into the vertical, generating a salinity stratification of order $1.3 \times 10^{-9}$ psu $m^{-1}$ $s^{-1}$. Thus, it would take 18 days for a 0.1 psu gradient to develop in the top 50 m. The *Roemmich et al.* [1994] salinity-driven tilting may have contributed to the barrier layer formations during these events, and may have helped initiate the stratification/shear flow tilting feedback. However, alone, it could not account for the sheared zonal flow and barrier layer formations observed during these two WWBs.

**Acknowledgments.** The data presented in this analysis were provided through efforts of many individuals. In particular, we wish to thank R. Lukas (U. Hawaii), D. Tang (N. Taiwan U.), K. Kutsuwada (Tokai U.), B. Weisberg (U. South Florida), T. Delcroix (IRD), and the officers and crews of the ships which maintained the moored arrays. Analysis and graphics were produced using the Ferret program developed at NOAA/PMEL. This is NOAA/PMEL publication #2381.

## References

Anderson, S. P., R. A. Weller, and R. B. Lukas, Surface buoyancy forcing and the mixed layer of the western Pacific warm pool: Observations and 1-d model results, *J. Clim., 9*, 3056–3085, 1996.

Ando, K., and M. J. McPhaden, Variability of surface layer hydrography in the tropical Pacific Ocean, *J. Geophys. Res., 102*, 23,063–23,078, 1997.

Cronin, M. F., and W. S. Kessler, Seasonal and interannual modulation of mixed layer variability at 0°, 110°W, *Deep-Sea Res. I, 49*, 1–17, 2002.

Cronin, M. F., and M. J. McPhaden, Diurnal cycle of rainfall and surface salinity in the western Pacific warm pool, *Geophys. Res. Lett., 26*, 3465–3468, 1999.

Cronin, M. F., and M. J. McPhaden, The upper ocean heat balance in the western equatorial Pacific warm pool during September–December 1992, *J. Geophys. Res., 102*, 8533–8553, 1997.

Cronin, M. F., and M. J. McPhaden, Upper ocean salinity balance in the western equatorial Pacific, *J. Geophys. Res., 103*, 27,567–27,587, 1998.

Cronin, M. F., M. J. McPhaden, and R. H. Weisberg, Wind-forced reversing jets in the western equatorial Pacific, *J. Phys. Oceanogr., 30*, 657–676, 2000.

Delcroix, T., C. Hénin, V. Porte, and P. Arkin, Precipitation and sea-surface salinity in the tropical Pacific, 1974–1989, *Deep-Sea Res., 43*, 1123–1141, 1996.

Delcroix, T., C. Hénin, F. Masia, and D. Varillon, Three decades of in situ sea surface salinity measurements in the tropical Pacific Ocean, CD-ROM, version 1.0, Insitut de Recherche pour le Développement, Nouvelle-Calédonie, 2000.

Freitag, H. P., M. McCarty, C. Nosse, R. Lukas, M. J. McPhaden, and M. F. Cronin, COARE SEACAT data: Calibration and quality control procedures, *NOAA Tech. Memo. ERL PMEL-115*, Seattle, WA, 89 pp., 1999.

Godfrey, J. S., R. A. Houze, Jr., R. H. Johnson, R. Lukas, J.-L. Rdelsperger, A. Sumi, and R. Weller, Coupled Ocean-Atmosphere Response Experiment (COARE): An interim report, *J. Geophys. Res., 103*, 14,395–14,450, 1998.

Godfrey, J. S., and E. J. Lindstrom, The heat budget of the equatorial western Pacific surface mixed layer, *J. Geophys. Res., 94*, 8007–8017, 1989.

Helber, R. W., and R. H. Weisberg, Equatorial upwelling in the western Pacific warm pool, *J. Geophys. Res., 106,* 8989–9003, 2001.

Hénin, C., Y. Du Penhoat, and M. Ioualalen, Observations of sea surface salinity in the western Pacific fresh pool: Large-scale changes in 1992–1995, *J. Geophys. Res., 103*, 7523–7536, 1998.

Ioualalen, M., and C. Hénin, Thermohaline variability of the western tropical Pacific during 1995–1998: On the erosion/reconstitution of the fresh pool, *J. Geophys. Res., 106,* 6869–6879, 2001.

Lukas, R., and E. Lindstrom, The mixed layer of the western equatorial Pacific Ocean. *J. Geophys. Res. Suppl., 96*, 3343–3357, 1991.

Madden, R. A., and P. R. Julian, Observations of the 40-50-day tropical oscillation—A review, *Mon. Weather Rev., 122*, 814–837, 1994.

McPhaden, M. J., A. J. Busalacchi, R. Cheney, J. R. Donguy, K. S. Gage, D. Halpern, M. Ji, P. Julian, G. Meyers, G. T. Mitchum, P. P. Niiler, J. Picaut, R. W. Reynolds, N. Smith, and K. Takeuchi, The Tropical Ocean Global Atmosphere (TOGA) observing system: a decade of progress, *J. Geophys. Res., 103*, 14,169–14,240, 1998.

McPhaden, M. J., H. P. Freitag, S. P. Hayes, B. A. Taft, Z. Chen, and K. Wyrtki, The response of the equatorial Pacific Ocean to a westerly wind burst in May 1986, *J. Geophys. Res., 93*, 10,589–10,603, 1988.

McPhaden, M. J., F. Bahr, Y. Du Penhoat, E. Firing, S. P. Hayes, P. P. Niiler, P. L. Richardson, and J. M. Toole, The response of the western equatorial Pacific Ocean to westerly wind bursts during November 1989 to January 1990, *J. Geophys. Res., 97*, 14,289–14,303, 1992.

Moore, D. W., and S. G. H. Philander, Modeling the equatorial oceanic circulation, In: *The Sea*, Vol. VI, Wiley Interscience, New York, 319–361, 1977.

Reynolds, R. W., and T. M. Smith, Improved global sea surface temperature analyses using optimum interpolation, *J. Clim., 7*, 929–948, 1994.

Roemmich, D., M. Morris, W. R. Young, and J. R. Donguy, Fresh equatorial jets, *J. Phys. Oceanogr., 24*, 540–558, 1994.

Smyth, W. D., P. O. Zavialov, and J. N. Moum, Decay of turbulence in the upper ocean following sudden isolation from surface forcing, *J. Phys. Oceanogr., 27*, 810–822, 1997.

Sprintall, J., and M. J. McPhaden, Surface layer variations observed in multiyear time series measurements from the western equatorial Pacific, *J. Geophys. Res., 99,* 963–979, 1994.

Sprintall, J., and M. Tomczak, Evidence of the barrier layer in the surface layer of the tropics, *J. Geophys. Res., 97*, 7305–7316, 1992.

Soloviev, A. and R. Lukas, Observation of spatial variability of diurnal thermocline and rain-formed halocline in the western Pacific warm pool, *J. Phys. Oceanogr., 26*, 2529–2538, 1996.

Stommel, H., Wind-drift near the equator, *Deep-Sea Res., 6*, 298–302, 1960.

Vialard, J., and P. Delecluse, An OGCM study for the TOGA decade. Part I: Role of salinity in the physics of the western Pacific fresh pool, *J. Phys. Oceanogr., 28*, 1071–1088, 1998a.

Vialard, J., and P. Delecluse, An OGCM study for the TOGA decade. Part II: Barrier layer formation and variability, *J. Phys. Oceanogr., 28*, 1089–1106, 1998b.

Webster, P. J., and R. Lukas, TOGA COARE: The Coupled Ocean-Atmosphere Response Experiment, *Bull. Am. Meteorol. Soc., 73*, 1377–1417, 1992.

Wijesekera, H. W., and M. C. Gregg, Surface layer response to weak winds, westerly bursts, and rain squalls in the western Pacific Warm Pool, *J. Geophys. Res., 101*, 977–997, 1996.

Wijesekera, H. W., C. A. Paulson, and A. Huyer, The effect of rainfall on the surface layer during a westerly wind burst in the western equatorial Pacific, *J. Phys. Oceanogr., 29*, 612–632, 1999.

Xie, P., and P. Arkin, Global precipitation: a 17-year monthly analysis based on gauge observations, satellite estimates, and numerical model outputs, *Bull. Am. Meteorol. Soc., 78*, 2539–2558, 1997.

Yoshida, K., A theory of the Cromwell Current and equatorial upwelling, *J. Oceanogr. Soc. Jpn., 15*, 154–170, 1959.

You, Y., Salinity variability and its role in the barrier-layer formation during TOGA-COARE, *J. Phys. Oceanogr., 25*, 2778–2807, 1995.

Zhang, C., and M. J. McPhaden, Intraseasonal surface cooling in the equatorial western Pacific, *J. Clim., 13*, 2261–2276, 2000.

M. F. Cronin, M. J. McPhaden, NOAA/Pacific Marine Environmental Laboratory, 7600 Sand Point Way NE, Seattle, WA 98115 USA. (cronin@pmel.noaa.gov)

(Received _____.)

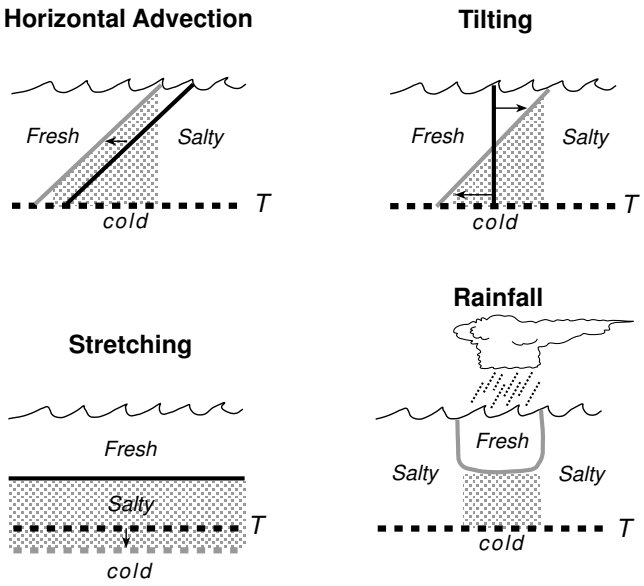


**Figure 1.** Cartoons illustrating the mechanisms by which barrier layers can form and grow corresponding to terms (1) horizontal advection, (3) tilting, (4) stretching, and (5) rainfall, in equations (2) and (4). The initial halocline and thermocline are indicated by respectively a black solid line and a black dashed line. The resulting halocline and thermocline are indicated by respectively, a grey solid line and grey dashed line. Stippling indicates the resulting barrier layer.

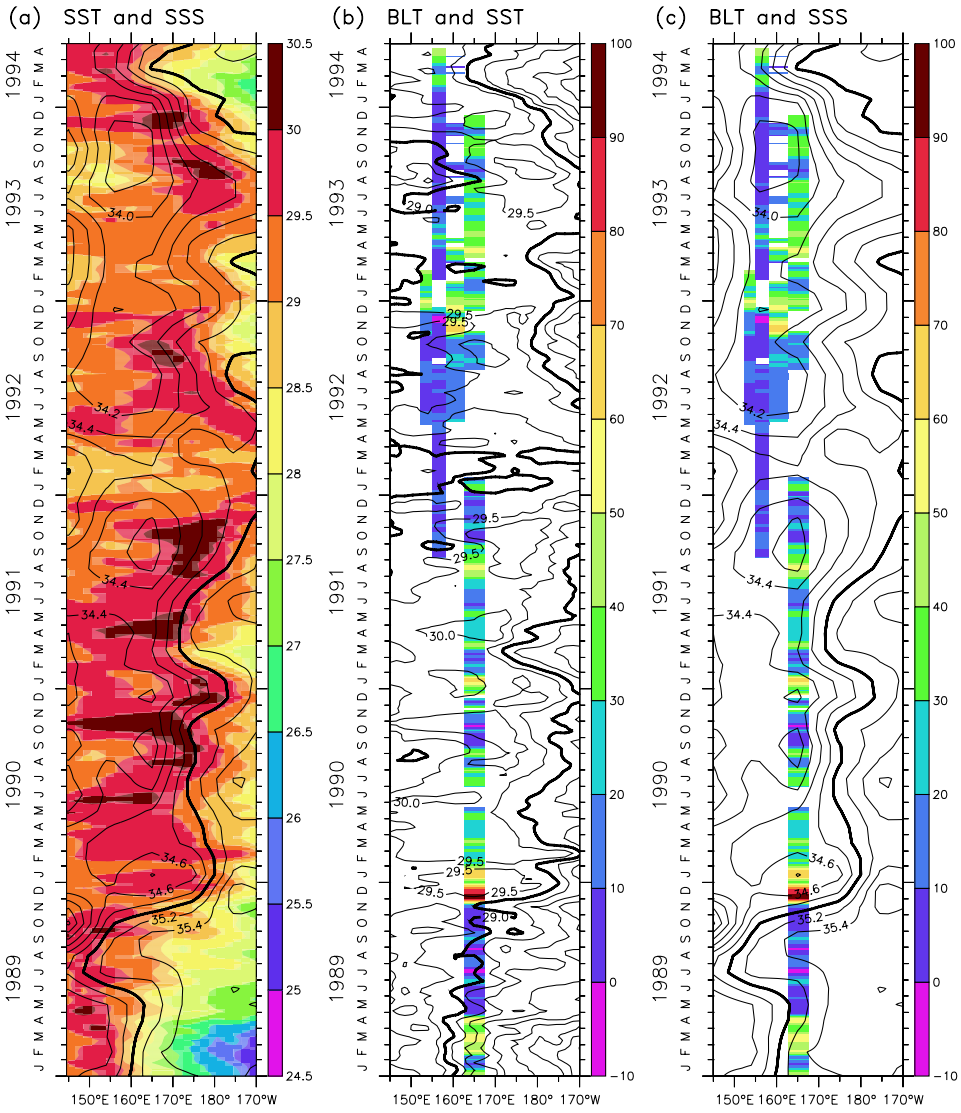


**Figure 2.** (a) *Reynolds and Smith* [1994] sea surface temperature (SST) (shaded) and *Delcroix et al.* [2000] gridded sea surface salinity (SSS) (contoured). (b) 15-day smoothed barrier layer thickness (BLT) computed from moored data (pixel time series) and *Reynolds and Smith* SST (contoured). (c) BLT (pixel time series) and gridded SSS (contoured). SST contour interval (CI) is 0.5°C and dark contour is 29.0°C; SSS CI is 0.2 psu and dark contour is 35.0 psu.

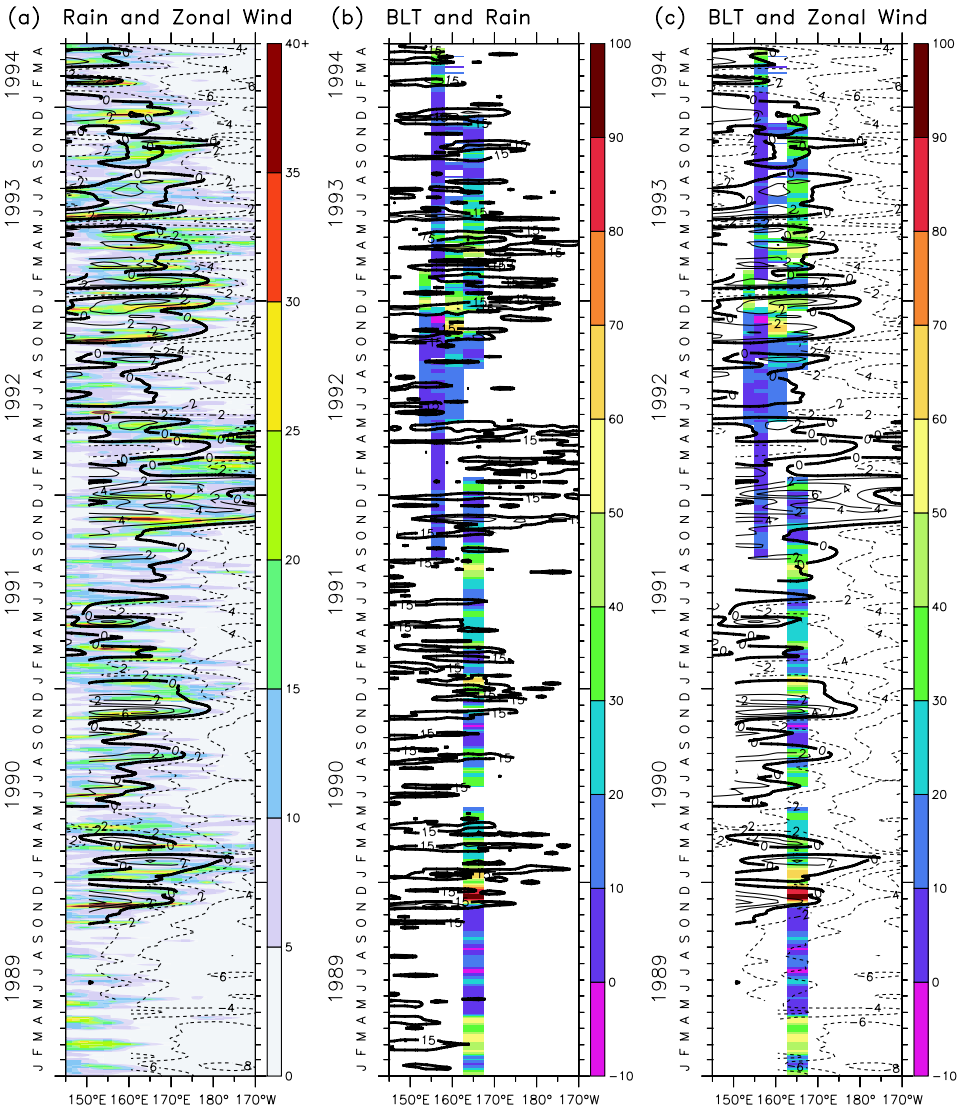


**Figure 3.** (a) *Xie and Arkin* [1997] pentad rain rates (shaded) and TAO gridded zonal winds (contoured). (b) BLT and *Xie and Arkin* rain rates. (c) BLT and TAO zonal wind. Zonal wind CI is 2 m $s^{-1}$ and zero contour is dark; rain rate CI is 15 mm $day^{-1}$ and dark contour is 15 mm $day^{-1}$.

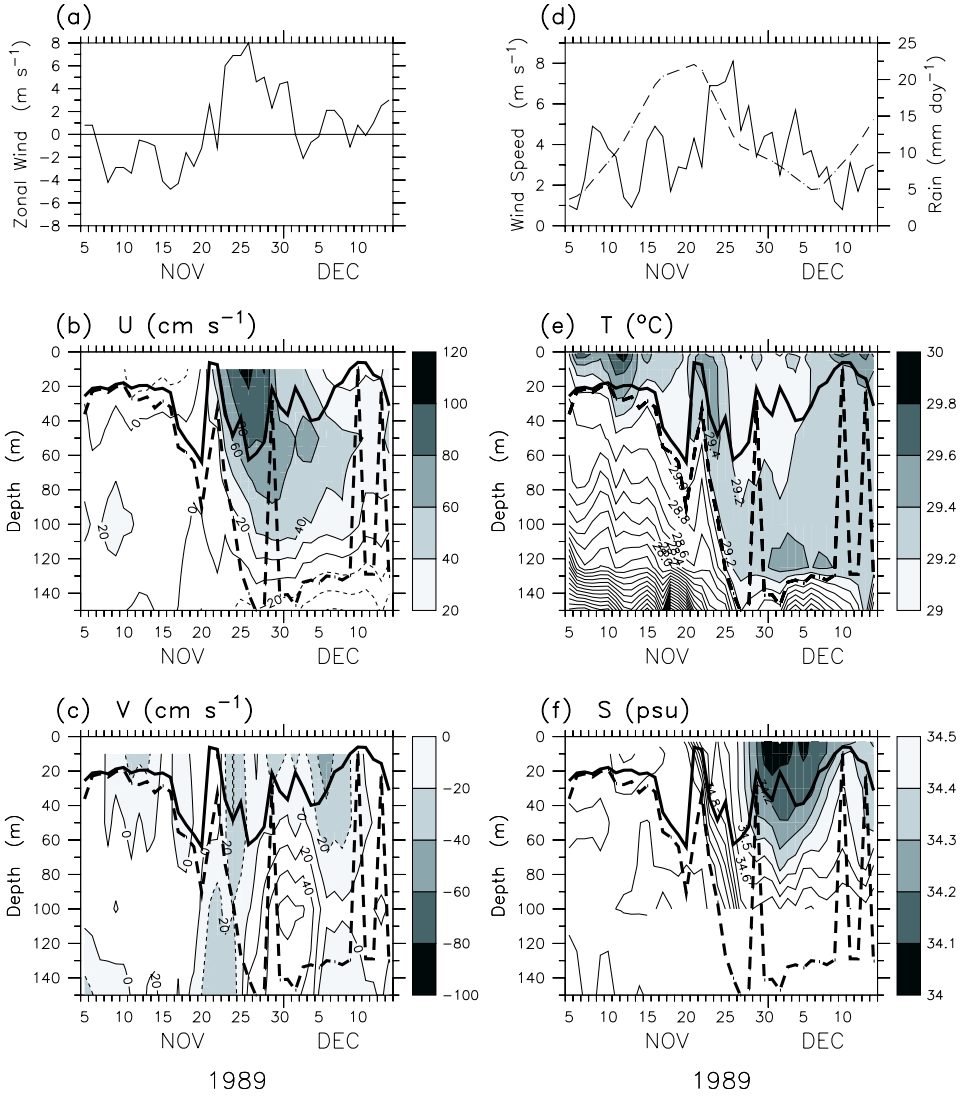


**Figure 4.** Moored 0°, 165°E daily averaged time series from November 5, 1989 through December 14, 1989: (a) zonal wind (in units m s$^{-1}$), (b) zonal velocity (CI is 20 cm s$^{-1}$, eastward flow above 20 cm s$^{-1}$ shaded), (c) meridional velocity (CI is 20 cm s$^{-1}$, southward flow shaded), (d) wind speed (solid line, in units m s$^{-1}$), (e) temperature (CI is 0.2°C, temperatures higher than 29°C shaded), and (f) salinity (CI is 0.1 psu, salinity less than 34.5 psu shaded). Mixed layer depth (solid thick line) and isothermal mixed layer depth (dashed thick line) as defined by (5–6) are superimposed on panels (b–c) and (e–f). *Xie and Arkin* pentad rain rate at 0°, 165°E (in units mm day$^{-1}$) is shown as a dashed line in panel (d).

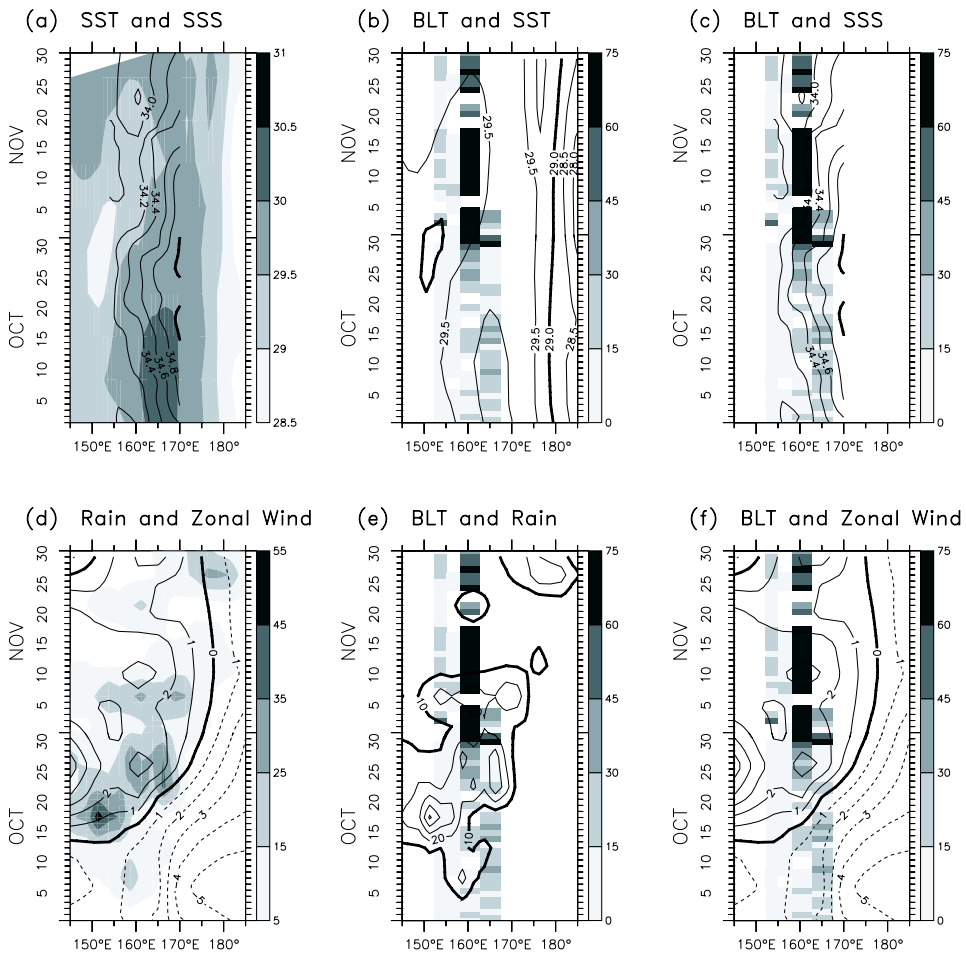


**Figure 5.** Surface fields along equator during October and November 1992. (a) *Reynolds and Smith* SST (shaded) and SSS from moorings along equator at 154°E, 156°E, 160.5°E, 165°E, and 170°E (contoured). (b) BLT and Reynolds and Smith SST. (c) BLT and moored SSS. (d) *Xie and Arkin* pentad rainfall rates (shaded) and TAO gridded zonal winds (contoured). (e) BLT and *Xie and Arkin* rainfall rates. (f) BLT and TAO zonal winds. SST CI is 0.5°C and dark contour is 29.0°C. SSS CI is 0.2 psu and dark contour is 35.0 psu. Only positive BLT values are shown. Zonal wind CI is 1 m $s^{-1}$, westerly winds are solid lines, easterly winds are dashed, and the zero contour is dark. Rain rate CI is 10 mm $day^{-1}$ and dark contour is 10 mm $day^{-1}$.

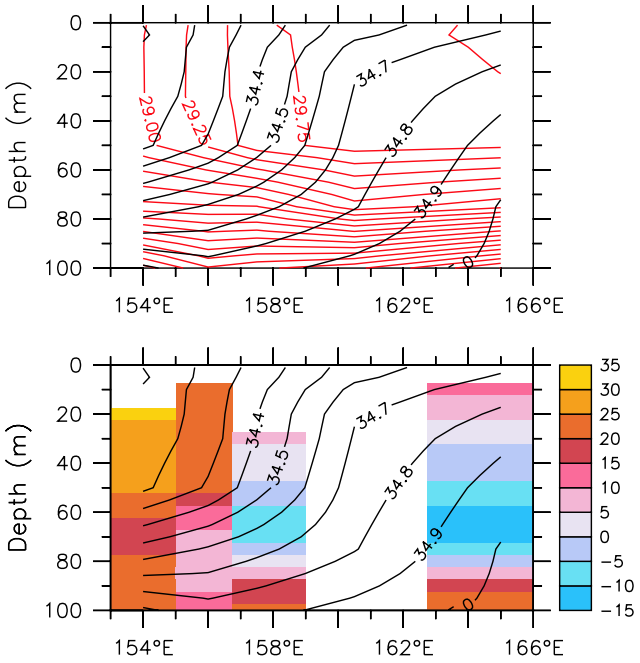


**Figure 6.** Time-averaged zonal-depth sections between 0°, 154°E and 0°, 165°E for October 27–November 1, 1992. Upper panel: Subsurface temperature (red contours, CI is 0.25°C) and subsurface salinity (black contours, CI is 0.1 psu). Lower panel: Zonal currents (shaded, in units cm $s^{-1}$) and subsurface salinity (black contours, CI is 0.1 psu).